14A.3   **MORE ON THE BOWEN RATIO OVER SATURATED SURFACES**

Edgar L Andreas[1*], Rachel E. Jordan[2], Larry Mahrt[3], and Dean Vickers[4]

[1]NorthWest Research Associates, Inc.; Lebanon, New Hampshire
[2]Jordan Environmental Modeling, PC; Hanover, New Hampshire
[3]NorthWest Research Associates, Inc.; Corvallis, Oregon
[4]College of Earth, Ocean, and Atmospheric Sciences, Oregon State University; Corvallis, Oregon

1. INTRODUCTION

The Bowen ratio partitions the total turbulent surface heat flux into contributions from sensible heat (H_s) and latent heat (H_L):

$$Bo = \frac{H_s}{H_L}. \qquad (1.1)$$

As a result, the Bowen ratio occurs repeatedly throughout micrometeorology (e.g., Panofsky and Dutton 1984, p. 92f., 132, 186; Garratt 1992, p. 36, 130f.; Lewis 1995).

A common use for the Bowen ratio is in the *Bowen ratio and energy budget method* (e.g., Fleagle and Businger 1980, p. 290f.; Brutsaert 1982, p. 210; Arya 1988, p. 191; Stull 1988, p. 274). We represent the surface energy budget as

$$0 = Q_{S\downarrow} - Q_{S\uparrow} + Q_{L\downarrow} - Q_{L\uparrow} + G - H_s - H_L. \quad (1.2)$$

Here, Q_S and Q_L are shortwave and longwave radiative fluxes at the surface; a down-arrow represents incoming radiation; and an up-arrow, outgoing radiation. G is the conductive flux up to the surface from below. In (1.2), the radiative terms are all taken as positive; H_s and H_L are positive when the flux is from surface to air. Hence, positive terms in (1.2) warm the surface; negative terms cool it.

If we represent the sum of the radiative terms as R_{net}, the net radiation, (1.1) and (1.2) let us partition the available energy ($R_{net} + G$) into sensible and latent heat fluxes:

$$H_s = \frac{Bo(R_{net} + G)}{1 + Bo}, \qquad (1.3a)$$

---

[*]*Corresponding author address:* Dr. Edgar L Andreas, NorthWest Research Associates, Inc. (Seattle Division), 25 Eagle Ridge, Lebanon, NH 03766-1900; e-mail: eandreas@nwra.com.

$$H_L = \frac{R_{net} + G}{1 + Bo}. \qquad (1.3b)$$

That is, this method provides the turbulent fluxes without turbulence measurements.

Other uses of the Bowen ratio are in interpreting sonic anemometer data (Schotanus et al. 1983; Andreas et al. 1998) and in specifying the Obukhov length, the stratification parameter in the atmospheric surface layer, when the latent heat flux is unknown (e.g., Busch 1973; Andreas 1992). Wesley (1976), Kunkel and Walters (1983), and Andreas (1988) showed how electromagnetic propagation in the surface layer is sensitive to the Bowen ratio.

In bulk flux algorithms, the turbulent surface heat fluxes are usually parameterized as (e.g., Fairall et al. 1996; Andreas et al. 2008, 2010a, 2010b)

$$H_s = \rho c_p C_{Hr} S_r (\Theta_s - \Theta_r), \qquad (1.4a)$$

$$H_L = \rho L_v C_{Er} S_r (Q_s - Q_r). \qquad (1.4b)$$

Here, ρ is the air density; c_p, the specific heat of air at constant pressure; L_v, the latent heat of vaporization or sublimation; S_r, an effective wind speed at reference height r; Θ_r and Q_r, the potential temperature and specific humidity at r; and C_{Hr} and C_{Er}, the transfer coefficients for sensible heat and latent heat, respectively, appropriate for height r.

Finally in (1.4), Θ_s and Q_s are the potential temperature and specific humidity at the surface. In this work, we exclusively discuss so-called *saturated surfaces*. For these, Q_s is computed as the saturation specific humidity at temperature Θ_s. Typical saturated surfaces include the open ocean, sea ice, large lakes, extensive snow fields, and large glaciers.

From (1.4) and (1.1), we can also represent the Bowen ratio as

$$Bo = \frac{c_p C_{Hr}(\Theta_s - \Theta_r)}{L_v C_{Er}(Q_s - Q_r)} . \qquad (1.5)$$

Thus, if we know the gradients $\Theta_s - \Theta_r$ and $Q_s - Q_r$ and have measured either H_s or H_L, we can calculate the other flux by knowing the Bowen ratio. Notice also that the signs of $\Theta_s - \Theta_r$ and $Q_s - Q_r$ dictate the signs of H_s, H_L, and Bo.

Over saturated surfaces, the Bowen ratio is tightly constrained. Philip (1987) theoretically established the constraint on the Bowen ratio for the case $H_s > 0$ and $H_L > 0$ under the assumption that the near-surface humidity is not above its saturation value—that is, no fog. Andreas (1989; see also Philip 1989) extended Philip's ideas to also formulate constraints for the cases $H_s < 0$, $H_L < 0$ and $H_s < 0$, $H_L > 0$. Andreas and Cash (1996) subsequently tested all three of these constraints using data collected over the open ocean, over sea ice, over a large lake, and over snow-covered ground. Andreas and Jordan (2011) continued this type of analysis but used two large datasets collected over sea ice.

Here, to the Andreas and Jordan (2011) datasets, we add a comparably sized dataset comprising 13 distinct sets collected over various open ocean regions. In our combined dataset, surface temperatures range from $-44°$ to $32°C$ and largely dictate the value of the Bowen ratio. For well over 90% of the time in all the individual datasets, the measured sensible and latent heat fluxes collect into one of three regimes: $H_s > 0$ and $H_L > 0$; $H_s < 0$ and $H_L < 0$; and $H_s < 0$ and $H_L > 0$.

As in Andreas and Cash (1996), we define a Bowen ratio indicator function Bo_* that depends approximately exponentially on surface temperature. In each of the three heat flux regimes, $|Bo| \sim Bo_*$. Moreover, the data, on average, support the three constraints formulated by Philip (1987), Andreas (1989), and Andreas and Cash (1996). That is, when $H_s > 0$ and $H_L > 0$, $Bo \leq Bo_*$; when $H_s < 0$ and $H_L < 0$, $Bo \geq Bo_*$; and when $H_s < 0$ and $H_L > 0$, $Bo \approx -Bo_*$.

2. CONTRAINTS ON THE BOWEN RATIO

Yet another way to formulate the sensible and latent heat fluxes in the atmospheric surface layer is with the turbulent diffusivities for temperature and humidity, K_θ and K_q, respectively (cf. Dyer 1974; Philip 1987):

$$H_s = -\rho c_p K_\theta(z)\partial\Theta/\partial z , \qquad (2.1a)$$

$$H_L = -\rho L_v K_q(z)\partial Q/\partial z , \qquad (2.1b)$$

where z is the height. There is no compelling evidence that K_θ and K_q are different (e.g., Högström 1996); consequently, Eqs. (2.1) reduce to

$$\frac{H_s}{H_L} = Bo = \frac{c_p}{L_v \partial Q/\partial\Theta} . \qquad (2.2)$$

Because H_s and H_L are constants with height in the atmospheric surface layer over a horizontally homogeneous surface, $\partial Q/\partial\Theta$ must be also. We can thus evaluate it at the surface, which has temperature Θ_s. (The physical surface temperature and the potential temperature Θ_s are commonly taken to be the same over surfaces like snow, sea ice, and the open ocean.) Moreover, if the surface is saturated, $\partial Q/\partial\Theta|_{\Theta_s}$ is the relation for the saturation specific humidity. Hence, following Philip (1987), we define

$$Bo_* \equiv \frac{c_p}{L_v \partial Q_{sat}/\partial\Theta}\bigg|_{\Theta_s} . \qquad (2.3)$$

Andreas and Cash (1996) give the equations that we use for calculating this quantity. Because the saturation vapor pressure used in calculating $\partial Q_{sat}/\partial\Theta$ depends weakly on surface salinity and barometric pressure, Bo_* does, too.

Figure 1 shows that Bo_* is a strong function of temperature because the saturation vapor pressure is an exponentially increasing function of temperature. Priestley and Taylor (1972) and Hicks and Hess (1977) used Bo_* to estimate the Bowen ratio and to predict evaporation over saturated surfaces. Raupach (2001) formulated a theory of equilibrium evaporation in terms of Bo_*. Jo et al. (2002) deduced a climatology for the Bowen ratio over the ocean from Bo_*.

On assuming, for the case when $H_s > 0$ and $H_L > 0$, that the humidity above a saturated surface is not above its saturation value, Philip (1987) deduced

$$\frac{\partial Q}{\partial\Theta} \geq \frac{\partial Q_{sat}}{\partial\Theta}\bigg|_{\Theta_s} . \qquad (2.4)$$
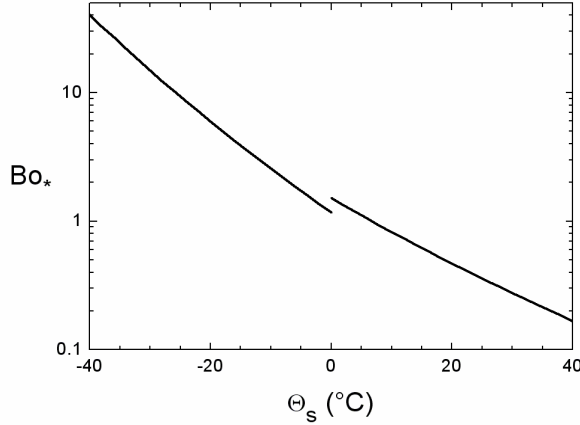
FIG.1. Bo_* from (2.3) as a function of surface temperature, Θ_s. For these calculations, the barometric pressure was 1000 mb and the surface salinity was zero. The discontinuity at $\Theta_s = 0\,°C$ occurs because the calculation uses the saturation vapor pressure over ice and the latent heat of sublimation for L_v for temperatures less than $0\,°C$ but the saturation over water and the latent heat of vaporization for temperatures above $0\,°C$.

Consequently, in this case, from (2.2)–(2.4),

$$Bo \leq Bo_* . \tag{2.5}$$

Panel a in Fig. 2 graphically demonstrates this argument. The heavy curved line is $Q_{sat}(\Theta)$. At Θ_s, the straight line tangent to the curve is $\partial Q_{sat} / \partial \Theta |_{\Theta_s}$. For $H_s > 0$ and $H_L > 0$, the air temperature and specific humidity must be in the sector indicated by the shading. Thus, $\partial Q / \partial \Theta \geq \partial Q_{sat} / \partial \Theta |_{\Theta_s}$ and $Bo \leq Bo_*$.

But besides being positive, both H_s and H_L can conceivably be negative or zero. Thus, there are nine combinations of H_s and H_L. Figure 2 depicts all of these combinations and highlights their implication for constraints on the Bowen ratio. Some combinations are forbidden under the assumption of a saturated surface but no super-saturation above the surface: namely, the cases in panels d, g, and h. The cases $H_s = 0$, $H_L > 0$ (panel b) and $H_s < 0$, $H_L = 0$ (panel f) are trivial because $Bo = 0$ for the former and $Bo = -\infty$ for the latter. In the case $H_s = 0$, $H_L = 0$ (panel e), Bo is undefined.

Using arguments as above for the $H_s > 0$, $H_L > 0$ case, Andreas (1989) showed that the $H_s < 0$, $H_L < 0$ case (panel i) also is constrained by

Bo_*. But now the constraint (2.4) becomes

$$\frac{\partial Q}{\partial \Theta} \leq \left. \frac{\partial Q_{sat}}{\partial \Theta} \right|_{\Theta_s} . \tag{2.6}$$

As a result, when $H_s < 0$ and $H_L < 0$,

$$Bo \geq Bo_* . \tag{2.7}$$

Finally, Andreas and Cash (1996) suggested that, for the case $H_s < 0$, $H_L > 0$ (panel c),

$$Bo \approx -Bo_* . \tag{2.8}$$

Over the saturated surfaces that they studied, Andreas and Cash (1996) found that three regimes in Fig. 2 dominate: the cases $H_s > 0$, $H_L > 0$; $H_s < 0$, $H_L < 0$; and $H_s < 0$, $H_L > 0$ (panels a, i, and c). Over 90% of the measured fluxes that they analyzed fell into one of these combinations.

Andreas and Cash (1996) also found that the constraints (2.5), (2.7), and (2.8) were useful in quantifying the Bowen ratio in these three dominant flux regimes. We repeat some of their analyses here using much larger datasets collected over both sea ice and the open ocean.

3. DATA

Table 1 summarizes the datasets that we use in this study. Two large sets were collected over sea ice: one in the Antarctic on Ice Station Weddell; and the second, in the Arctic during SHEBA, the experiment to study the Surface Heat Budget of the Arctic Ocean (Uttal et al. 2002). The other 13 datasets were obtained over the open ocean from a ship, on a platform, and from low-flying aircraft (flight level less than 50 m). The "Reference" column in Table 1 lists citations that provide additional information on the datasets. In addition, Mahrt et al. (2012) and Andreas et al. (2012) recently analyzed other aspects of the open ocean sets.

The "Number of Observations" column in Table 1 shows the number of individual measurements that each dataset contributed to our analysis. A useful set of observations had to provide three pieces of information: measurements of Θ_s, H_s, and H_L. A key feature of each dataset in Table 1 is that both H_s and H_L were obtained from eddy-covariance measurements.
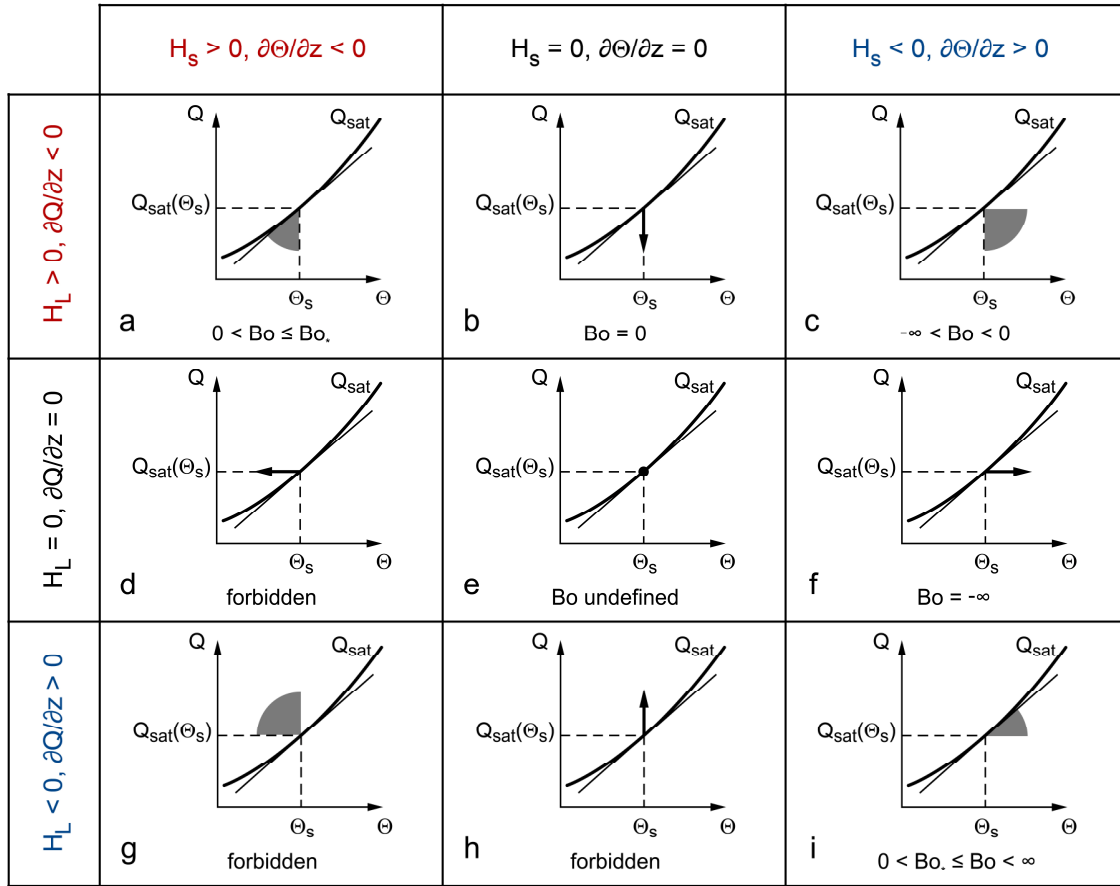
For the open ocean sets, usually much more

FIG 2. Nine combinations of sensible (H_s) and latent (H_L) heat fluxes and what they say about the Bowen ratio (Bo). The flux is assumed to be down the respective gradient: $\partial\Theta/\partial z$ for sensible heat, and $\partial Q/\partial z$ for latent heat. In each panel, the thicker, curved line is $Q_{sat}(\Theta)$, the relation for saturation in specific humidity. Θ_s is the surface temperature. The thin, straight line tangent to the Q_{sat} curve at Θ_s is $\left.\partial Q_{sat}/\partial\Theta\right|_{\Theta_s}$ and is used in defining Bo_*, (2.3). The shaded areas show where the Q and Θ values above the surface must lie for the given gradients. Heavy arrows indicate that Q or Θ must lie along these lines. The dot in panel e shows the only values that Q and Θ can assume. Any values of Q and Θ that lie above the $Q_{sat}(\Theta)$ line are forbidden by our assumption that the near-surface humidity is not above saturation.

data than listed in Table 1 were available; but we screened these data to focus on the best measurements for our analysis. First, as explained by Andreas et al. (2012), we are concerned that the aircraft flux data in stable stratification may be biased because of vertical flux divergence. Therefore, for our analysis of the Bowen ratio, we used the same criteria that Andreas et al. developed: We retained only the data collected in unstable and weakly stable conditions, $-\infty < z_{ac}/L \leq 0.1$, where z_{ac} is the aircraft flight level and L is the measured Obukhov length.

Second, in high winds over the ocean, heat transfer from sea spray droplets augments the interfacial heat fluxes that are parameterized as (1.4) (Andreas and DeCosmo 2002; Andreas et al. 2008; Andreas 2010). In effect, this spray-mediated heat transfer can cause a countergradient flux (Andreas 2011) that thereby confuses the definition of the Bowen ratio given by (1.5). Spray effects, however, appear to be negligible when the 10-m, neutral-stability wind speed, U_{N10}, is less than about 13 m s^{-1} (e.g.,

Table 1. The datasets used in this study. The "Number of Observations" is the number of cases left after the screening described in the text. The first two sets are the sea ice sites; the remaining datasets were collected over the open ocean. The "Reference" provides additional details on a dataset. Mahrt et al. (2012) and Andreas et al. (2012) also provide more information on the open ocean sets.

Dataset	Number of Observations	Platform/Location	Reference
Ice Station Weddell	1031	Tower on sea ice, western Weddell Sea	Andreas et al. (2004, 2005)
SHEBA	2859	Tower on sea ice, Beaufort Gyre, Arctic Ocean	Persson et al. (2002), Andreas et al. (2010a, 2010b)
FASTEX	136	*R/V Knorr*, transect across the North Atlantic	Persson et al. (2005)
GFDex	11	FAAM BAE 146 aircraft, Irminger Sea and Denmark Strait	Petersen and Renfrew (2009)
HEXOS	109	Meetpost Noordwijk platform, North Sea	DeCosmo (1991)
CARMA4	455	CIRPAS Twin Otter, off coast of southern California	
CBLAST-weak	592	Long-EZ aircraft, Martha's Vineyard, MA	Edson et al. (2007)
GOTEX	312	NCAR C-130, Gulf of Tehuantepec	Romero and Melville (2010)
MABLEB	24	CIRPAS Twin Otter, off Monterey, CA	
Monterey	475	CIRPAS Twin Otter, off Monterey, CA	Mahrt and Khelif (2010)
POST	178	CIRPAS Twin Otter, off Monterey, CA	
RED	344	CIRPAS Twin Otter, east of Oahu, Hawaii	Anderson et al. (2004)
SHOWEX Nov '97	373	Long-EZ aircraft, off coast of Virginia and North Carolina	Sun et al. (2001)
SHOWEX Nov '99	580	Long-EZ aircraft, off coast of Virginia and North Carolina	Sun et al. (2001)
TOGA COARE	742	NCAR Electra, western equatorial Pacific Ocean	Sun et al. (1996), Vickers and Esbensen (1998)

Table 2. Dominant heat flux regimes. The three H_s, H_L columns list the percentage of the total cases in each H_s and H_L flux regime. The last column is the percentage of total cases that occurred in these three regimes.

Dataset	$H_s > 0$ $H_L > 0$ (%)	$H_s < 0$ $H_L < 0$ (%)	$H_s < 0$ $H_L > 0$ (%)	Total, these three cases (%)
Ice Station Weddell	31.6	43.6	15.3	90.5
SHEBA	36.4	31.0	25.8	93.2
FASTEX	86.8	1.5	10.3	98.6
GFDex	100.0	0.0	0.0	100.0
HEXOS	89.9	0.0	10.1	100.0
CARMA4	70.8	7.2	18.9	96.9
CBLAST-weak	56.2	24.8	15.4	96.4
GOTEX	68.0	0.0	32.0	100.0
MABLEB	79.2	0.0	20.8	100.0
Monterey	81.3	0.0	13.0	94.3
POST	77.5	5.6	12.4	95.5
RED	99.1	0.0	0.9	100.0
SHOWEX Nov '97	77.5	0.0	22.5	100.0
SHOWEX Nov '99	83.1	2.4	12.4	97.9
TOGA COARE	96.1	0.0	3.2	99.3

Andreas et al. 2008). Hence, from the open ocean datasets, we retain for analysis only data for which $U_{N10} \leq 13$ m s^{-1}. This screening reduced, in particular, the FASTEX, GFDex, and GOTEX datasets dramatically (by 50% or more) because these experiments sought high winds.

4. FLUX REGIMES

To demonstrate the conceptual utility of Fig. 2, we sorted each dataset into flux regimes. Table 2 summarizes the results.

In each of the 15 datasets, the three flux regimes $H_s > 0$, $H_L > 0$; $H_s < 0$, $H_L < 0$; and $H_s < 0$, $H_L > 0$ constitute more than 90% of the observed cases. Over the ocean, the $H_s > 0$, $H_L > 0$ regime is dominant by far (cf. Hsu 1998), and the $H_s < 0$, $H_L < 0$ regime is rare.

Over sea ice, the $H_s > 0$, $H_L > 0$ and $H_s < 0$,

$H_L < 0$ regimes are comparable, although the Ice Station Weddell data may bias this picture. SHEBA was a year-long deployment, so these data should not be biased by seasonal changes. Ice Station Weddell, however, was an autumn and early winter experiment when stable stratification (i.e., $H_s < 0$) was dominant.

Table 2 thus confirms what Fig. 2 suggests. Of the nine possible combinations for H_s and H_L, several are forbidden by the assumption that the near-surface humidity is not above its saturation value. Other combinations, though permissible, are meteorologically rare: namely, cases when either H_s or H_L is zero.

5. Bo-Bo$_*$ RELATIONS

Figures 3, 4, and 5 show *Bo* versus *Bo$_*$* for all

the datasets summarized in Table 1. Between the sea ice and ocean datasets, we have over 4700 observations in the $H_s > 0$, $H_L > 0$ regime (Fig. 3) and almost 1500 observations in both the $H_s < 0$, $H_L < 0$ (Fig. 4) and $H_s < 0$, $H_L > 0$ (Fig. 5) regimes. The only comparable previous analysis was by Andreas and Cash (1996), and they had only about 1200 observations total.

Because these are log-log plots, a first option would be to represent the Bowen ratio as

$$Bo = \alpha \, Bo_*^\beta . \qquad (5.1)$$

In each figure, however, the bin-averaged points suggest a slope that tends to parallel the 1:1 line. That is, $|Bo| \propto Bo_*$. Hence, in each of Figs. 3 to 5, the solid line shows the best fit through the data for which β in (5.1) is one. For the $H_s > 0$, $H_L > 0$ plot (Fig. 3), we obtain

$$Bo = (0.38 \pm 0.02) \, Bo_* ; \qquad (5.2)$$

for the $H_s < 0$, $H_L < 0$ plot (Fig. 4),

$$Bo = (3.14 \pm 0.28) \, Bo_* ; \qquad (5.3)$$

and for the $H_s < 0$, $H_L > 0$ plot (Fig. 5),

$$Bo = -(0.58 \pm 0.06) \, Bo_* . \qquad (5.4)$$

Equation (5.2) has the same coefficient that Andreas and Cash (1996) obtained for the $H_s > 0$, $H_L > 0$ case. Thus, we again confirm Philip's (1987) original theoretical result that $Bo \le Bo_*$ when $H_s > 0$ and $H_L > 0$, the surface is saturated, but the near-surface humidity is not above its saturation value.

The coefficient in (5.3) is about three times larger than in Andreas and Cash's (1996) analysis. But they had fewer than 170 observations in this $H_s < 0$, $H_L < 0$ regime and only 15 observations collected over the open ocean. Equation (5.3) is thus a more accurate result. Our new result and Andreas and Cash's confirms Andreas's (1989) conclusion that $Bo \ge Bo_*$ when $H_s < 0$ and $H_L < 0$.

Our (5.4) is similar to Andreas and Cash's (1996) result for the $H_s < 0$, $H_L > 0$ regime: Our coefficient is –0.58; theirs is –0.32. Consequently, we, too, support the suggestion by Andreas and Cash that $Bo \approx -Bo_*$ in the $H_s < 0$ and $H_L > 0$ regime.

Because of the scatter in the data in Figs. 3–5, a reasonable single alternative to (5.2)–(5.4) for
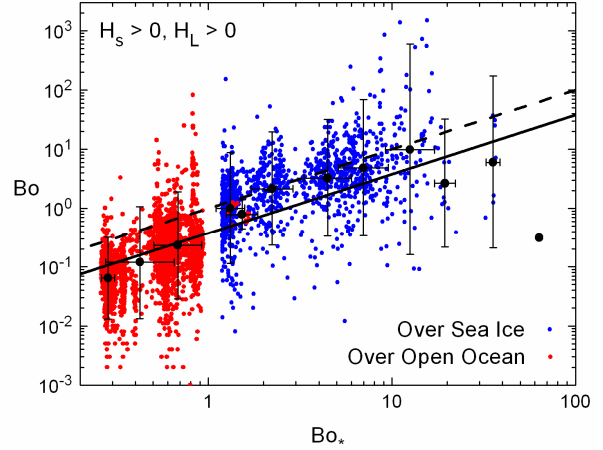

FIG. 3. Values of the Bowen ratio calculated from the measured values of H_s and H_L in the datasets in Table 1 are compared with corresponding values of Bo_* computed from (2.3). The plot is for cases when $H_s > 0$ and $H_L > 0$. The two colors distinguish between data collected over sea ice and over the open ocean. The bigger black circles are averages in Bo_* bins, where there are four bins per decade. The error bars are ±2 standard deviations in the bin populations. There are two bin averages for Bo_* between 1 and 2: one for the ocean cases, and one for the sea ice cases. The black dashed line is 1:1; the solid black line is (5.2).

predicting the Bowen ratio in the three dominant H_s and H_L regimes is that

$$|Bo| \approx Bo_* \qquad (5.5)$$

in each regime.

6. DISCUSSION AND CONCLUSIONS

With roughly 8000 eddy-covariance observations over both sea ice and the open ocean where surface temperatures ranged from −44° to 32 °C, this is, to our knowledge, the most encompassing survey to date of the Bowen ratio over saturated surfaces.

Though nine combinations of H_s and H_L are conceivable—both H_s and H_L can be positive, negative, or zero—three combinations dominate our data: $H_s > 0$, $H_L > 0$; $H_s < 0$, $H_L < 0$; and $H_s < 0$, $H_L > 0$. In the sea ice datasets, these three combinations constitute over 90% of the observations. In the open ocean datasets, they always represent at least 94% of the observations.
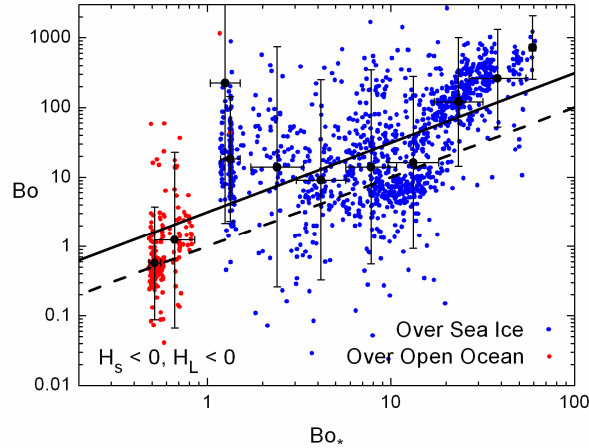
FIG. 4. As in Fig. 3, except this shows the cases for which $H_s < 0$ and $H_L < 0$. The solid black line is (5.3).

FIG. 5. As in Fig. 3, except this shows the cases for which $H_s < 0$ and $H_L > 0$. The solid black line is (5.4).

Furthermore, in these three regimes, the average behavior of the resulting Bowen ratio ($= H_s/H_L$) is constrained by the Bowen ratio indicator Bo_* [see (2.3)]. For the $H_s > 0$, $H_L > 0$ regime, we confirm Philip's (1987) postulated constraint: $Bo \le Bo_*$. For the $H_s < 0$, $H_L < 0$ regime, we likewise confirm Andreas's (1989) conclusion: $Bo \ge Bo_*$. Finally, our data in the $H_s < 0$, $H_L > 0$ regime support Andreas and Cash's (1996) suggestion: $Bo \approx -Bo_*$. Equations (5.2)–(5.4) represent these results.

We envision several possible uses for our results. One is as a quality control on measurements or model estimates of H_s and H_L. The values obtained should have a climatology similar to those in Table 2. The inferred Bowen ratio should also depend on surface temperature as predicted in (5.2)–(5.4). In fact, (5.2)–(5.4) can provide an estimate of the Bowen ratio in any of the many applications that require it.

In particular, (5.2)–(5.4) provide partitioning of the sensible and latent heat fluxes and, thus, could be key components for estimating the surface energy budget from satellite data over saturated surface like the ocean, sea ice, or the Greenland or Antarctic ice sheets. For example, Bentamy et al. (2003) demonstrated that satellite sensors can provide estimates of wind speed and $Q_s - Q_r$ (also Liu 1988) over the ocean; H_L follows immediately from (1.4b). H_s could then easily derive from (1.1) and (5.2)–(5.4) because surface temperature— and, thus, Bo_*—is a common satellite measurement.
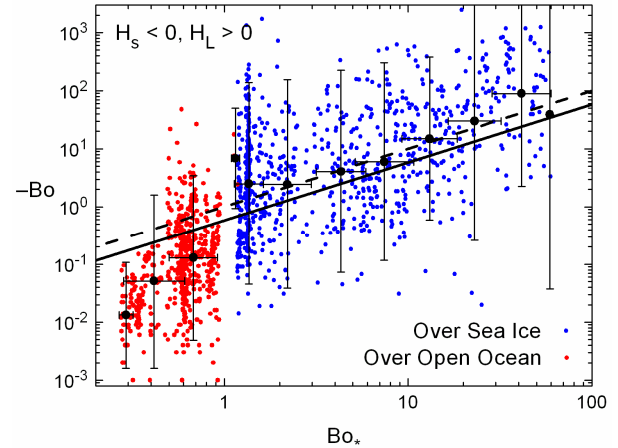
Moreover, satellites can provide estimates of

the radiation terms in (1.2). Over sea ice, the remaining term in the surface energy budget, the conductive flux G, could be estimated with a simple heat conduction equation and satellite measurements of the water and sea ice surface temperatures. Therefore, with an estimate of the Bowen ratio through Bo_*, (1.3) provide the remaining turbulence terms in the surface energy budget.

7. ACKNOWLEDGMENTS

8. REFERENCES

Anderson, K., and 20 coauthors, 2004: The RED Experiment: An assessment of boundary

layer effects in a trade winds regime on microwave and infrared propagation over the sea. *Bull. Amer. Meteor. Soc.*, **85**, 1355–1365.

Andreas, E. L, 1988: Estimating C_n^2 over snow and sea ice from meteorological data. *J. Opt. Soc. Amer. A*, **5**, 481–495.

——, 1989: Comments on "A physical bound on the Bowen ratio." *J. Appl. Meteor.*, **28**, 1252–1254.

——, 1992: Uncertainty in a path-averaged measurement of the friction velocity u_*. *J. Appl. Meteor.*, **31**, 1312–1321.

——, 2010: Spray-mediated enthalpy flux to the atmosphere and salt flux to the ocean in high winds. *J. Phys. Oceanogr.*, **40**, 608–619.

——, 2011: Fallacies of the enthalpy transfer coefficient over the ocean in high winds. *J. Atmos. Sci.*, **68**, 1435–1445.

——, and B. A. Cash, 1996: A new formulation for the Bowen ratio over saturated surfaces. *J. Appl. Meteor.*, **35**, 1281–1289.

——, and J. DeCosmo, 2002: The signature of sea spray in the HEXOS turbulent heat flux data. *Bound.-Layer Meteor.*, **103**, 303–333.

——, and R. E. Jordan, 2011: The Bowen ratio over sea ice. Extended abstract, *11th Conf. on Polar Meteorology and Oceanography*, Boston, MA, 2–5 May 2011, American Meteorological Society, paper 1.2, 9 pp.

——, R. J. Hill, J. R. Gosz, D. I. Moore, W. D. Otto, and A. D. Sarma, 1998: Statistics of surface-layer turbulence over terrain with metre-scale heterogeneity. *Bound.-Layer Meteor.*, **86**, 379–408.

——, R. E. Jordan, and A. P. Makshtas, 2004: Simulations of snow, ice, and near-surface atmospheric processes on Ice Station Weddell. *J. Hydrometeor.*, **5**, 611–624.

——, ——, and ——, 2005: Parameterizing turbulent exchange over sea ice: The Ice Station Weddell results. *Bound.-Layer Meteor.*, **114**, 439–460.

——, P. O. G. Persson, and J. E. Hare, 2008: A bulk turbulent air-sea flux algorithm for high-wind, spray conditions. *J. Phys. Oceanogr.*, **38**, 1581–1596.

——, T. W. Horst, A. A. Grachev, P. O. G. Persson, C. W. Fairall, P. S. Guest, and R. E. Jordan, 2010a: Parameterising turbulent exchange over summer sea ice and the marginal ice zone. *Quart. J. Roy. Meteor. Soc.*, **136**, 927–943.

——, P. O. G. Persson, R. E. Jordan, T. W. Horst, P. S. Guest, A. A. Grachev, and C. W. Fairall, 2010b: Parameterizing turbulent exchange over sea ice in winter. *J. Hydrometeor.*, **11**, 87–104.

——, L. Mahrt, and D. Vickers, 2012: A new drag relation for aerodynamically rough flow over the ocean. *J. Atmos. Sci.*, to appear.

Arya, S. P., 1988: *Introduction to Micrometeorology*. Academic Press, 307 pp.

Bentamy, A., K. B. Katsaros, A. M. Mestas-Nuñez, W. M. Drennan, E. B. Forde, and H. Roquet, 2003: Satellite estimates of wind speed and latent heat flux over the global ocean. *J. Climate*, **16**, 637–656.

Brutsaert, W. H., 1982: *Evaporation into the Atmosphere: Theory, History, and Applications*. D. Reidel, 299 pp.

Busch, N. E., 1973: On the mechanics of turbulence. *Workshop on Micrometeorology*, D. A. Haugen, Ed., American Meteorological Society, 1–65.

Dyer, A. J., 1974: A review of flux-profile relationships. *Bound.-Layer Meteor.*, **7**, 363–372.

DeCosmo, J., 1991: Air-sea exchange of momentum, heat and water vapor over whitecap sea states. Ph.D. dissertation, University of Washington, 212 pp.

Edson, J., and 28 coauthors, 2007: The Coupled Boundary Layers and Air–Sea Transfer Experiment in low winds. *Bull. Amer. Meteor. Soc.*, **88**, 341–356.

Fairall, C. W., E. F. Bradley, D. P. Rogers, J. B. Edson, and G. S. Young, 1996: Bulk parameterization of air-sea fluxes for Tropical Ocean-Global Atmosphere Coupled-Ocean Atmosphere Response Experiment. *J. Geophys. Res.*, **101**, 3747–3764.

Fleagle, R. G., and J. A. Businger, 1980: *An Introduction to Atmospheric Physics*. 2nd ed. Academic Press, 432 pp.

Garratt, J. R., 1992: *The Atmospheric Boundary Layer*. Cambridge University Press, 316 pp.

Hicks, B. B., and G. D. Hess, 1977: On the Bowen ratio and surface temperature at sea. *J. Phys. Oceanogr.*, **7**, 141–145.

Högström, U., 1996: Review of some basic characteristics of the atmospheric surface layer. *Bound.-Layer Meteor.*, **78**, 215–246.

Hsu, S. A., 1998: A relationship between the Bowen ratio and sea-air temperature difference under unstable conditions at sea. *J. Phys. Oceanogr.*, **28**, 2222–2226.

Jo, Y.-H., X.-H. Yan, J. Pan, M.-X. He, and W. T. Liu, 2002: Calculation of the Bowen ratio in the tropical Pacific using sea surface temperature data. *J. Geophys. Res.*, **107**

(C9), 3134, doi:10.1029/2001JC001150.

Kunkel, K. E., and D. L. Walters, 1983: Modeling the diurnal dependence of the optical refractive index structure parameter. *J. Geophys. Res.*, **88** (C15), 10,999–11,004.

Lewis, J. M., 1995: The story behind the Bowen ratio. *Bull. Amer. Meteor. Soc.*, **76**, 2433–2443.

Liu, W. T., 1988: Moisture and latent heat flux variabilities in the tropical Pacific derived from satellite data. *J. Geophys. Res.*, **93** (C6), 6749–6760.

Mahrt, L., and D. Khelif, 2010: Heat fluxes over weak SST heterogeneity. *J. Geophys. Res.*, **115**, D11103, doi:10.1029/2009JD013161.

——, D. Vickers, E. L Andreas, and D. Khelif, 2012: Sensible heat flux in near-neutral conditions over the sea. *J. Phys. Oceanogr.*, to appear.

Panofsky, H. A., and J. A. Dutton, 1984: *Atmospheric Turbulence: Models and Methods for Engineering Applications*. John Wiley and Sons, 397 pp.

Persson, P. O. G., C. W. Fairall, E. L Andreas, P. S. Guest, and D. K. Perovich, 2002: Measurements near the Atmospheric Surface Flux Group tower at SHEBA: Near-surface conditions and surface energy budget. *J. Geophys. Res.*, **107** (C10), 8045, doi:10.1029/2000JC000705.

——, J. E. Hare, C. W. Fairall, and W. D. Otto, 2005: Air-sea interaction processes in warm and cold sectors of extratropical cyclonic storms observed during FASTEX. *Quart. J. Roy. Meteor. Soc.*, **131**, 877–912.

Petersen, G. N., and I. A. Renfrew, 2009: Aircraft-based observations of air-sea fluxes over Denmark Strait and the Irminger Sea during high wind speed conditions. *Quart. J. Roy. Meteor. Soc.*, **135**, 2030–2045.

Philip, J. R., 1987: A physical bound on the Bowen ratio. *J. Climate Appl. Meteor.*, **26**, 1043–1045.

——, 1989: Reply. *J. Appl. Meteor.*, **28**, 1255.

Priestley, C. H. B., and R. J. Taylor, 1972: On the assessment of surface heat flux and evaporation using large-scale parameters. *Mon. Wea. Rev.*, **100**, 81–92.

Raupach, M. R., 2001: Combination theory and equilibrium evaporation. *Quart. J. Roy. Meteor. Soc.*, **127**, 1149–1181.

Romero, L., and W. K. Melville, 2010: Airborne observations of fetch-limited waves in the Gulf of Tehuantepec. *J. Phys. Oceanogr.*, **40**, 441–465.

Stull, R. B., 1988: *An Introduction to Boundary Layer Meteorology*. Kluwer, 666 pp.

Schotanus, P., F. T. M. Nieuwstadt, and H. A. R. De Bruin, 1983: Temperature measurement with a sonic anemometer and its application to heat and moisture fluxes. *Bound.-Layer Meteor.*, **26**, 81–93.

Sun, J., J. F. Howell, S. K. Esbensen, L. Mahrt, C. M. Greb, R. Grossman, and M. A. LeMone, 1996: Scale dependence of air-sea fluxes over the Western Equatorial Pacific. *J. Atmos. Sci.*, **53**, 2997–3012.

——, D. Vandemark, L. Mahrt, D. Vickers, T. Crawford, and C. Vogel, 2001: Momentum transfer over the coastal zone. *J. Geophys. Res.*, **106**, 12,437–12,488.

Uttal, T., and 27 coauthors, 2002: Surface Heat Budget of the Arctic Ocean. *Bull. Amer. Meteor. Soc.*, **83**, 255–275.

Vickers, D., and S. K. Esbensen, 1998: Subgrid surface fluxes in fair weather conditions during TOGA COARE: Observational estimates and parameterization. *Mon. Wea. Rev.*, **126**, 620–633.

Wesley, M. L., 1976: The combined effect of temperature and humidity fluctuations on refractive index. *J. Appl. Meteor.*, **15**, 43–49.